IEEE Photonics Journal
An IEEE Photonics Society Publication

Open Access

Polarization-Insensitive Electro-Absorption Modulator Based on Graphene-Silicon Nitride Hybrid Waveguide

Volume 13, Number 3, June 2021

Wei Chen
Xiaojian Fan
Pengfei Li
Yang Gao
Lanting Ji
Xiaoqiang Sun
Daming Zhang

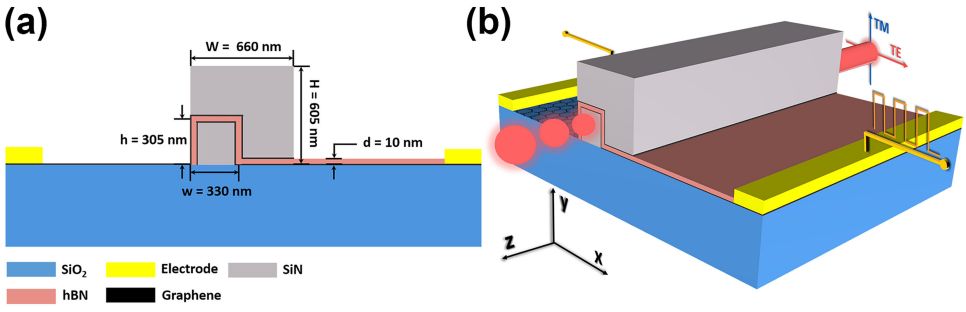

(a) Cross-sectional and (b) three-dimensional (3D) view of the proposed graphene/SiN electro-absorption modulator.

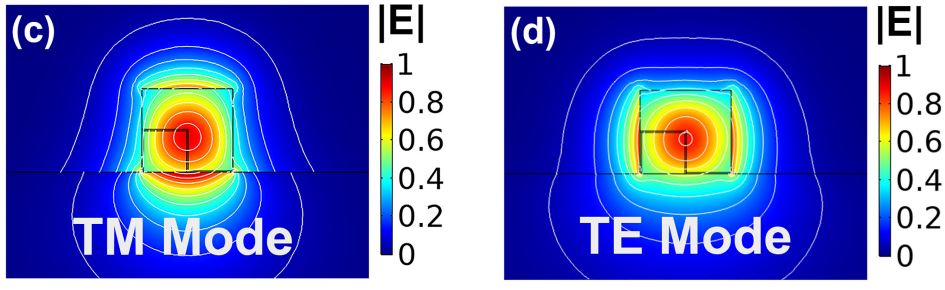

Modal profile of (c) TM mode and (d) TE mode supported by the hybrid graphene/SiN waveguide.

DOI: 10.1109/JPHOT.2021.3075204

IEEE photonics SOCIETY

IEEE

Polarization-Insensitive Electro-Absorption Modulator Based on Graphene-Silicon Nitride Hybrid Waveguide

Wei Chen,[1] Xiaojian Fan,[1] Pengfei Li,[1] Yang Gao,[1] Lanting Ji,[2] Xiaoqiang Sun,[1] and Daming Zhang[1]

[1]State Key Laboratory of Integrated Optoelectronics, College of Electronic Science & Engineering, Jilin University, Changchun 130012, China
[2]Institute of Marine Science and Technology, Shandong University, Qingdao 250100, China

DOI:10.1109/JPHOT.2021.3075204

Manuscript received February 22, 2021; accepted April 20, 2021. Date of publication April 23, 2021; date of current version May 7, 2021. This work was supported in part by the National Key Research and Development Program of China under Grant 2019YFB2203001, in part by the National Natural Science Foundation of China under Grants 61675087 and 61875069, and in part by the Education Department of Jilin Province under Grant JJKH20190118KJ. Corresponding author: Xiaoqiang Sun (e-mail: sunxq@jlu.edu.cn).

Abstract: Wideband and polarization-insensitive operation are key issues for electro-optic modulators. An electro-absorption modulator based on graphene-silicon nitride hybrid waveguide has been proposed. Geometric parameters are investigated through finite element method to enhance the interaction between the optical mode and the graphene. For a 200-μm-long hybrid waveguide, a modulation depth (MD) of 20 dB can be obtained when Femi level varies from 0.2 to 0.6 eV. The MD difference between the transversal electric polarization and transversal magnetic polarization (△MD) can be restrained to 4×10^{-3} dB at 1550 nm. A low average △MD of 0.2 dB within the wavelength range from 1100 to 1645 nm can be obtained. The 3 dB-bandwidth of 53 GHz and a power consumption is 0.687 pJ/bit can be obtained. The proposed modulator has potentials for on-chip signal processing.

Index Terms: Graphene, silicon nitride, waveguide, polarization-insensitive.

1. Introduction

High performance electro-optic (EO) modulator is highly demanded in wideband optics communication networks [1]. The lithium niobite-based modulators are matured, but suffering from large footprint and relatively high modulation voltage [2]. III-V electro-absorption modulators offer small footprint, however, the insertion loss and thermal stability are still to be improved [3]. Transparent conductive oxide is also one of the promising materials for EO modulator [4]. Silicon modulators are compatible with CMOS technology, while facing the problem of low EO efficiency [5], and relatively high optical loss brought by surface roughness compared to the typical value of 0.1 dB/μm of silicon nitride (SiN) waveguide [6]. As has been reported, the refractive index difference between SiN and SiO_2 cladding is smaller than that of SOI waveguide, which allows a larger mode dimension that is beneficial to the light coupling. SiN waveguide that is also compatible with CMOS technology is

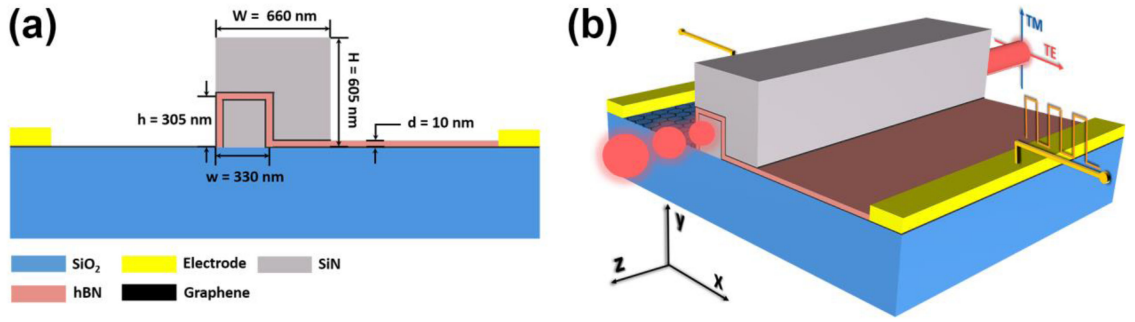

Fig. 1. (a) Cross-sectional and (b) three-dimensional (3D) view of the proposed graphene/SiN electro-absorption modulator.

favorable to the low-cost manufacturing [7]–[9]. Therefore, EO modulators incorporating graphene and SiN waveguide have been investigated [6, 10, 11].

Graphene is a single-atom layer material bonded by a carbon atom in a hexagonal form. This unique structure offers graphene excellent optical properties of controllable light absorption, high electron mobility (200,000 $cm^2V^{-1}s^{-1}$), uniform light absorption rate of 2.3% in a broadband [12]–[20]. These favorable properties offer the graphene good potentials in high speed, small footprint and low power consumption modulator applications [21]–[24]. In 2011, Liu *et al.* have reported a graphene optical modulator with a modulation depth (MD, the difference between "ON" state and "OFF" state) of 0.1 dB/μm [25]. A graphene optical modulator with graphene-isolation-graphene heterostructure is reported to have a MD of 0.16 dB/μm with a low power consumption of 1 pJ/bit [26]. A high 3 dB-bandwidth of 30 GHz for the graphene EO modulator has been demonstrated, too [27]. However, the extremely thin graphene flake is unfavorable to the strong interaction with the light field, posing a limitation on the graphene modulator performance. Therefore, the waveguide structure optimization [28, 29] or novel effect, such as plasmonic effect, have been introduced to enhance the interaction of graphene with the light field. Kim *et al.* proposed a modulator, in which the graphene is placed in the middle of optical waveguide to improve the interaction, and then the modulation depth [29]. Though plasmonic modulators offer high optical mode confinement and compact device size [30], the high optical loss is still the most challenge. Another issue for graphene applied in waveguide modulator is the polarization sensitivity, which originates from the low absorption rate with the electric polarization that is perpendicular to the graphene layer. Therefore, most reported works can only operate in transverse magnetic (TM) polarization or transverse electronic (TE) polarization, independently [31]. The introducing of additional polarization control structure is inevitable, which complicates the component. Thereby, a modulator that can provide independent-polarization and low loss operation is very desirable.

In this paper, a polarization-insensitive electro-absorption graphene modulator has been proposed. By constructing a heterostructure consisting of dual-graphene-covered substructure and SiN cap layer, TE and TM polarizations are simultaneously supported. With the enhancement of mode confinement in the hybrid waveguide, the quasi-equal interaction between graphene flakes and light mode at both vertical and lateral directions provide polarization independency and larger modulation depth. The waveguide geometry parameters are investigated and optimized based on finite element method. The mechanism of polarization-independence and broadband modulation is elaborated in detail. The proposed modulator design has potential in on-chip signal processing.

2. Configuration

2.1 Device Structure

The proposed electro-absorption modulator (EAM) based on hybrid graphene/SiN waveguide is shown in Fig. 1. Over the rectangle SiN stripe ($n_{SiN} = 1.98$) are two graphene flakes that is isolated

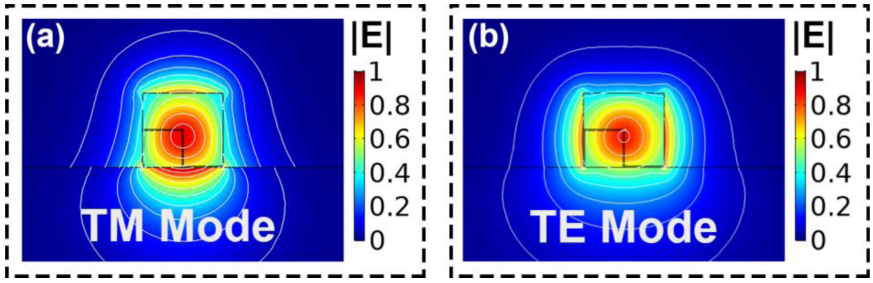

Fig. 2. Modal profile of (a) TM mode and (b) TE mode supported by the hybrid graphene/SiN waveguide.

by hBN spacer ($n_{hBN} = 1.98$). Both the rectangle SiN stripe and graphene flakes are half-covered by another top SiN layer. The Au contact forms the electrodes [32]. The isolation layer thickness is set to be 10 nm, which has been experimentally proved in reported graphene modulators [33, 34]. The whole structure is supported by a SiO_2 substrate ($n_{SiO2} = 1.45$).

Fig. 2(a) and (b) display the electric field distribution of TM and TE polarizations, respectively. Due to the effective refractive index symmetry in both x- and y-axis, both TE and TM polarizations can be supported by the proposed hybrid waveguide. Here, the graphene will interact with the tangential component (in-plane) of the electric field, leading to the interband transition. Thereby, only the longitudinal or transverse components will experience the absorption-induced optical loss. This polarization-dependent light absorption effect is determined by the tangential electric field component, as well as its overlap with the graphene flake. Therefore, graphene overlaid on the substructure in hybrid waveguide can have almost the same interaction with different polarization at certain waveguide dimension, and fulfill the polarization-insensitive modulation.

In order to better illustrate the optimization of the structural parameters and characterize the working performance of the proposed modulator, the mode power attenuation (MPA) and modulation depth (MD) are defined as follows

$$MPA = 40\pi(\log_{10}e)\mathrm{Im}(N_{\mathrm{eff}})/\lambda \tag{1}$$

$$\mathrm{MD} = [\mathrm{MPA}(OFF) - \mathrm{MPA}(ON)] * L \tag{2}$$

where $\mathrm{Im}(N_{\mathrm{eff}})$ is the imaginary part of the effective index, λ is the incident wavelength. In the following discussion, "ON" state refers to $\mu_c = 1$ eV, "OFF" state refers to $\mu_c = 0$ eV. For a certain modulation length L of 200 μm, MD is defined as the product of MPA difference at $\mu_c = 1$ and 0 eV, respectively.

2.2 Graphene Film

As shown in Fig. 1, two graphene layers together with the hBN isolation layer form a plate capacitor. Light absorption that can be adjusted by tuning the carrier accumulation is controlled by the applied external bias voltage. As has been reported [35], the graphene layer can be modeled as a 3D bulk material with a thickness of 0.33 nm (via the anisotropic dielectric constant or a two-dimensional surface structure). Commonly, a smaller grid size is more profitable in 3D simulations for accurate result. However, it implies longer calculation time and larger memories requirement. If the accuracy can be guaranteed, it is more desirable to model graphene as a two-dimensional (2D) layer. In this work, the graphene layer is considered as the dielectric with zero thickness. Benefit from the reduced number of meshes in this way, the decreased simulation time and accurate results can be obtained. The Kubo formula can well describe the surface conductivity of graphene σ_g as follows [36]

$$\sigma_g = \sigma_0 \left[\begin{array}{c} 1 + \frac{4\mu_c}{\pi}\frac{1}{\hbar(\Gamma_1 - j\omega)} + \frac{1}{\pi}\tan^{-1}\left(\frac{\hbar\omega - 2\mu_c}{\hbar\Gamma_2}\right) \\ -\frac{1}{\pi}\tan^{-1}\left(\frac{\hbar\omega + 2\mu_c}{\hbar\Gamma_2}\right) - \frac{1}{2\pi}\ln\left(\frac{(2\mu_c + \hbar\omega)^2 + (\hbar\Gamma_2)^2}{(2\mu_c - \hbar\omega)^2 + (\hbar\Gamma_2)^2}\right) \end{array} \right] \tag{3}$$

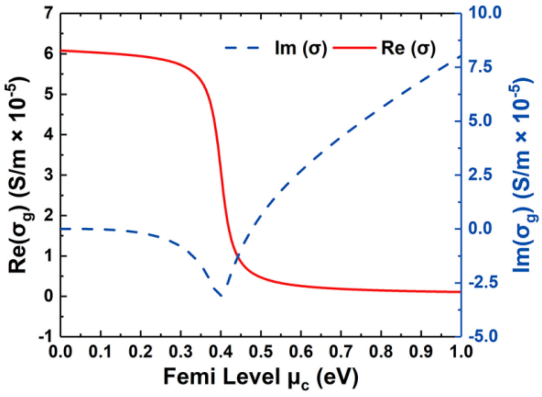

Fig. 3. Relationship between surface conductivity and Fermi level μ_c of graphene at the optical wavelength of 1550 nm.

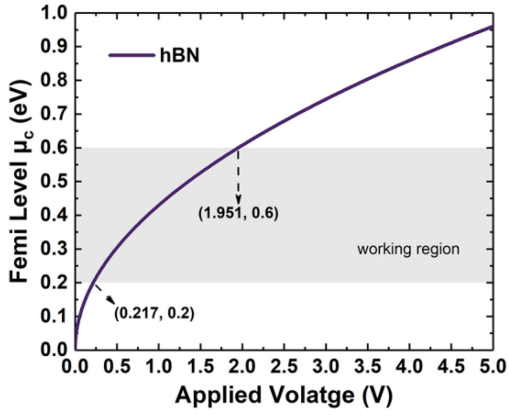

Fig. 4. Relationship between Fermi level μ_c and external applied voltage.

where σ_0 is the universal optical conductance that is about 60.8 μS, $\hbar$ is reduced Planck's constant, μ_c is the chemical potential (Femi level), ω is the optical frequency at the wavelength of 1550 nm, Γ_1 and Γ_2 are the charged particles scattering rate ($\Gamma = 1 / \tau$, where τ corresponds to the relaxation time), τ_1 is the intraband transition (1.2 ps) and τ_2 is interband transition (15 fs). As shown in Fig. 3, chemical potential μ_c can adjust the surface conductivity [19]. Eq. (4). expresses the correlation between μ_c and external bias voltage [19]

$$\mu_c = \hbar v_F \sqrt{\pi \eta \left| V_g - V_0 \right|} \tag{4}$$

where $v_F = 2.5 \times 10^6$ m/s is the Fermi velocity of graphene [37], $\eta = \varepsilon_r \varepsilon_0 / de$ is determined by a parallel plate capacitor model, d and ε_r are thickness and relative dielectric constant (permittivity) of the hBN isolation layer, respectively. As shown in Fig. 4, when the applied voltage varies from 0.217 to 1.951 V, μ_c shifts from 0.2 to 0.6 eV. It is worth noting that graphene exhibits a special physical property transition called the near-zero (ENZ) effect at μ_c (ENZ) $\approx$ 0.5 eV [38]. When μ_c is larger than μ_c (ENZ), graphene shows characteristics of a dielectric medium. While, graphene behaves like a metallic layer when μ_c is smaller than μ_c(ENZ), which will lead to strong light absorption.

3. Simulation and Discussion

In this section, the geometric parameters of proposed modulator are optimized by utilizing two-dimensional finite element method (FEM). The finite element method-based COMSOL Multiphysics

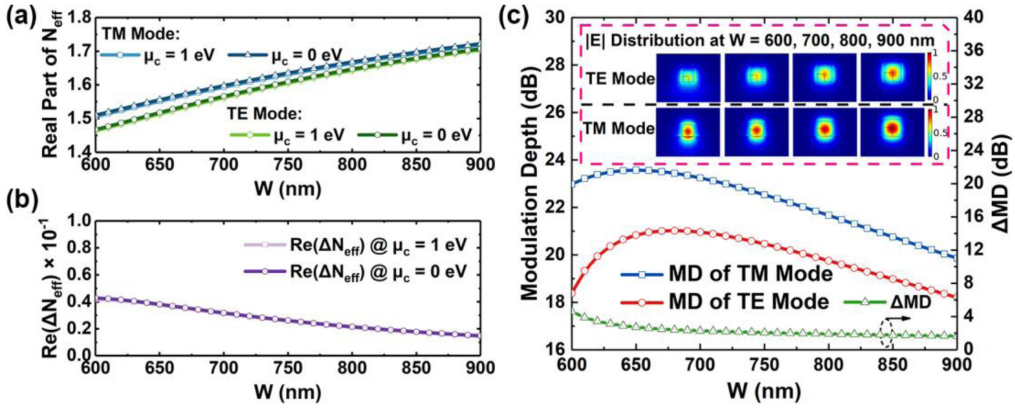

Fig. 5. (a) Re(N_{eff}), (b) Re(ΔN_{eff}), (c) MD and ΔMD of TM and TE modes versus W. The illustrations in (c) show the modal profiles at different W.

5.5 is used in the simulation. The free triangle meshes with the predefined size of 0.1 and 7.5×10^{-4} μm are adopted as the maximum and the minimum element, respectively. The scattering boundary condition is adopted to provide accurate results. The effective index of hybrid graphene/SiN waveguide is calculated at $\mu_c = 0$ and 1 eV, respectively. The MPA is evaluated based on Eq. (1). The polarization dependence is studied by comparing Re(ΔN_{eff}) defined by Eq. (5) and ΔMD determined by Eq. (6) under different geometric parameters.

$$\text{Re}\,(\Delta \text{Neff}) = \left|\text{Re}(\text{Neff})_{\text{TM}} - \text{Re}(\text{Neff})_{\text{TE}}\right| \tag{5}$$

$$\Delta\text{MD} = \left|\text{MD}_{\text{TM}} - \text{MD}_{\text{TE}}\right| \tag{6}$$

3.1 Effect of Waveguide Dimension W

As shown in Fig. 1, for structural symmetry, the hybrid waveguide is defined to have the same horizontal and vertical dimension, namely $W = H$. The height and width of the half-covered SiN stripe is chosen to be $w = h = H/2$, which is favorable to construct the symmetric effective index distribution for both TM mode and TE mode. Besides, it allows the symmetric interaction between the graphene and the square stripe in both the vertical and lateral direction. Re(N_{eff}), Re(ΔN_{eff}), MD, ΔMD of EAM as a function of waveguide dimension W is investigated. As shown in Fig. 5(a), when W increases from 600 to 900 nm, Re(N_{eff}) of TM mode increases from 1.50569 to 1.71841 at $\mu_c = 1$ eV, while increase from 1.51016 to 1.72221 at $\mu_c = 0$ eV. When W increases from 600 to 900 nm, Re(N_{eff}) of TE mode increases from 1.46384 to 1.70394 at $\mu_c = 1$ eV, while increase from 1.46738 to 1.70743 at $\mu_c = 0$ eV. As shown in Fig. 5(b), no remarkable Re(ΔN_{eff}) change can be observed over the W range. When W increases from 600 to 900 nm, Re(ΔN_{eff}) linearly decreases from 0.04185 to 0.01447 at $\mu_c = 1$ eV. Meanwhile, Re(ΔN_{eff}) linearly decreases from 0.04278 to 0.01478 at $\mu_c = 0$ eV. The modal power gradually focuses on the hybrid waveguide core with the increment of W (as illustrated in Fig. 5(c)). As illustrated in Fig. 5(c), the MD of TM mode rises up quickly with the increment of W, reaching to the peak of 23.55 dB at $W = 650$ nm. MD of TE mode reaches the peak of 20.95 dB at $W = 660$ nm. Both two modes decrease quasi-linearly with the increase of W. MD mainly relates to the graphene-light interaction strength in the hybrid waveguide. Besides, the MD difference between two modes (ΔMD) is below 2 dB and becomes stable when W is larger than 660 nm. In order to obtain strong modulation, W and H is chosen to be 660 nm.

3.2 Effect of Δh & ΔH

Due to the asymmetric waveguide structure, the interaction between the graphene layer and the electric field for TM and TE mode is different, which inevitably has impact on the polarization

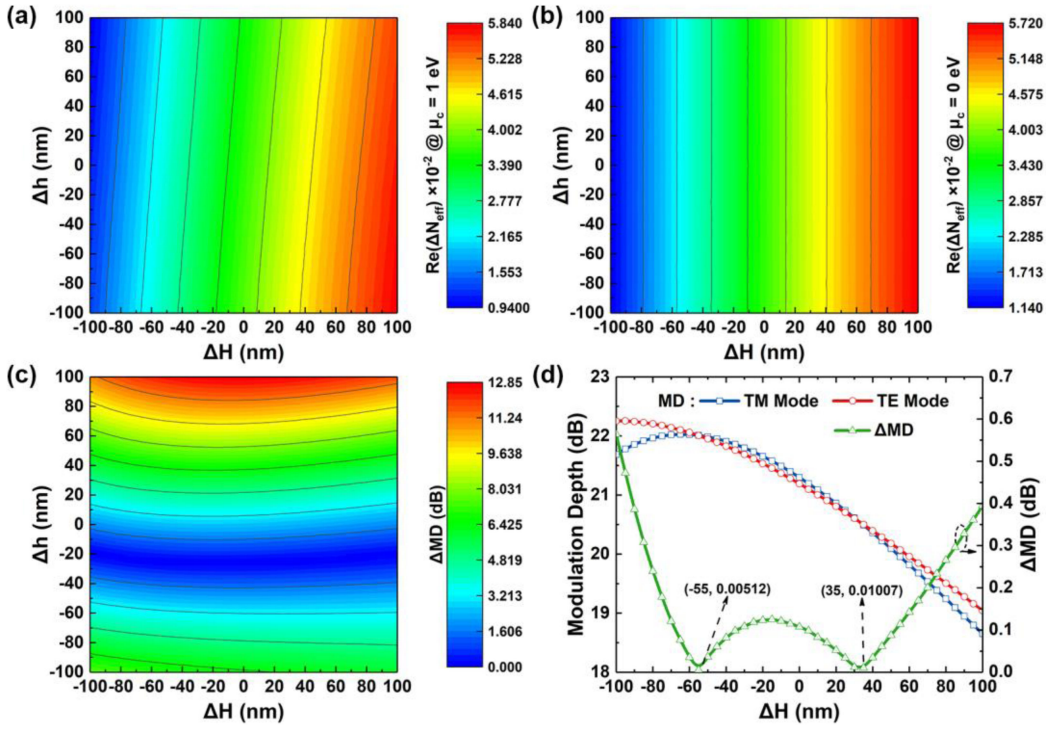

Fig. 6. (a) Re($\Delta N_{\rm eff}$) at $\mu_{\rm c} = 1$ eV, (b) Re($\Delta N_{\rm eff}$) at $\mu_{\rm c} = 0$ eV and (c) ΔMD versus waveguide height change ΔH and substructure height change Δh, (d) MD and ΔMD versus ΔH with fixed $\Delta h = -25$ nm.

independence. Theoretically, this effect is supposed to be alleviated by optimizing the waveguide geometric parameters. Hence, the influence of the change in waveguide height ΔH and substructure height Δh on Re($\Delta N_{\rm eff}$) and ΔMD of two modes is discussed. As shown in Fig. 6(A) and (b), the variation of ΔH and Δh has similar impact on Re($\Delta N_{\rm eff}$) at different $\mu_{\rm c}$. Re($\Delta N_{\rm eff}$) is insensitive to the change of h, but sensitive to ΔH. Re($\Delta N_{\rm eff}$) increases with the rising of H. The response difference of Re($\Delta N_{\rm eff}$) to the variation of ΔH and Δh mainly attributes to the fact that the Re($N_{\rm eff}$) of two modes is mainly affected by waveguide dimension.

Though the change of substructure height Δh has no impact on the height of complete waveguide H, it will affect the interaction strength between the graphene layer and the light field. As shown in Fig. 6(c), ΔMD is insensitive to the change of ΔH, however, declines with the decrement of Δh. The minimum ΔMD of 0.138 dB at $\Delta h =$ -25 nm indicates a balanced graphene-light interaction strength between two modes. Thereby, Δh is set to be -25 nm. As shown in Fig. 6(d), the MD of TM mode reaches to the peak value of 22.01 dB at $\Delta H = -65$ nm, and then decreases. In contrast, the MD of TE mode shows an approximately linear drop. The MDs of TM and TE modes have the same value at $\Delta H = -55$ and 35 nm, which indicates as two dips for ΔMD. Compared to the performance at $\Delta H = 35$ nm, a higher MD and a lower ΔMD can be obtained at $\Delta H = -55$ nm. Thereby, ΔH is chosen as -55 nm to optimize the polarization-insensitivity.

3.3 μ_c Response

The dependence of Re($N_{\rm eff}$), Re($\Delta N_{\rm eff}$) and MPA on the chemical potential $\mu_{\rm c}$ of graphene is also investigated. Fig. 7(a) shows that Re($N_{\rm eff}$) of TM mode firstly increases from 1.53486 to the peak of 1.53646 as $\mu_{\rm c}$ increases from 0 to 0.4 eV. Then it declines to 1.53058 when $\mu_{\rm c}$ increases to 1.0 eV. Similar Re($N_{\rm eff}$) change of TE mode can be observed, too. Furthermore, Re($\Delta N_{\rm eff}$) keeps at a low stage of around 2.33 $\times$ 10^{-2} when $\mu_{\rm c}$ varies from 0 to 1 eV. As depicted in Fig. 7(b), MPA of TM

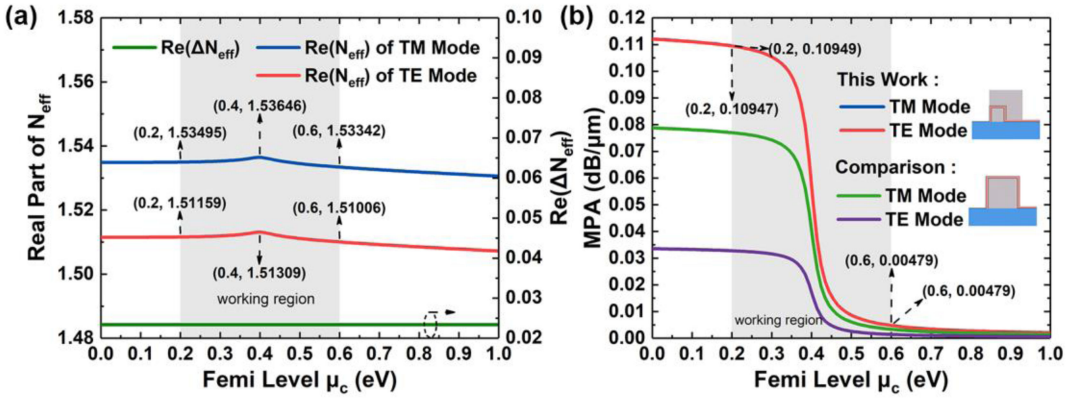

Fig. 7. Dependence of (a) Re(N_{eff}), Re(ΔN_{eff}), and (b) MPA of TM mode and TE mode on Femi level, insets in (b) show SiN waveguides that are fully covered and partly covered by graphene, respectively.

and TE modes show sharp decline when μ_c varies from 0.3 to 0.5 eV. Therefore, $\mu_c = 0.6$ eV is set to be the "ON" state, and $\mu_c = 0.2$ eV is set to be the "OFF" state. Accordingly, the MD for TM mode is evaluated to be 20.940 dB, which is very close to that of 20.936 dB for TE mode. As far as we know, this resulted $\triangle$MD of 4×10^{-3} dB is the smallest and two orders of magnitude lower than the minimum in reported single waveguide polarization-insensitive graphene modulators [39]–[45]. Furthermore, in the ON state, the propagation loss is calculated to be 0.985 dB for both modes. In addition, the coupling loss of 0.22 dB is introduced, which can be realized by adopting a SOI taper coupler [46]. Hence the insertion loss is estimated to be 1.425 dB (coupling loss $\times$ 2 + propagation loss).

Compared to graphene/SiN waveguide modulator with the graphene flakes directly cover on the 660 nm $\times$ 660 nm SiN square waveguide, as shown in the inset in Fig. 7(b), this hybrid waveguide design offers a much higher MD for both TM and TE modes. At the same time, the polarization insensitivity is kept. The MPA increases 42.16% for TM mode and 233.98% for TE mode, respectively. This significant increase in MD is attributed to the specially designed hybrid waveguide structure that enables graphene flakes to interact with higher intensity optical field. Furthermore, the proposed hybrid graphene/SiN waveguide electro-absorption modulator allows a smaller capacity, which is beneficial to a larger 3 dB-bandwidth.

3.4 Wavelength Dependence

To further study the bandwidth characteristics of proposed design, Re(N_{eff}), Re(ΔN_{eff}), MD and $\triangle$MD are investigated versus the optical wavelength λ. The optical 3 dB-bandwidth is introduced to estimate the band characteristics of the modulator. It is defined as the wavelength range that corresponds to the MD of any mode dropping by half (3 dB), when the wavelength is centered at 1550 nm. Fig. 8(a) shows a linear decrease of Re(N_{eff}) for both TM and TE modes, when λ is increasing. At $\lambda = 1100$ nm and $\mu_c = 0.6$ eV, a maximum Re(N_{eff}) of 1.71483 for TM mode and 1.70985 for TE mode can be observed. When $\lambda = 1100$ nm and $\mu_c = 0.2$ eV, a maximum Re(N_{eff}) of 1.7138 for TM mode and 1.70882 for TE mode is demonstrated. When $\lambda = 1717$ nm and $\mu_c = 0.6$ eV, a minimum Re(N_{eff}) of 1.47688 for TM mode and 1.4504 for TE mode can be observed, respectively. When $\lambda = 1750$ nm and $\mu_c = 0.2$ eV, a minimum Re(N_{eff}) of 1.47878 for TM mode and 1.45179 for TE mode is shown Fig. 8(a). In addition, a relatively low effective index difference with an average of 2.33×10^{-2} is achieved within the wavelength range from 1100 to 1717 nm. Fig. 8(b) shows the dependence of MD and $\triangle$MD on the optical wavelength. The MD of TM and TE modes firstly rises up and then reaches to the maximum at $\lambda = 1225$ nm. MDs then drop gradually as λ is increasing. To be mentioned, λ has a greater influence on the MD of TE

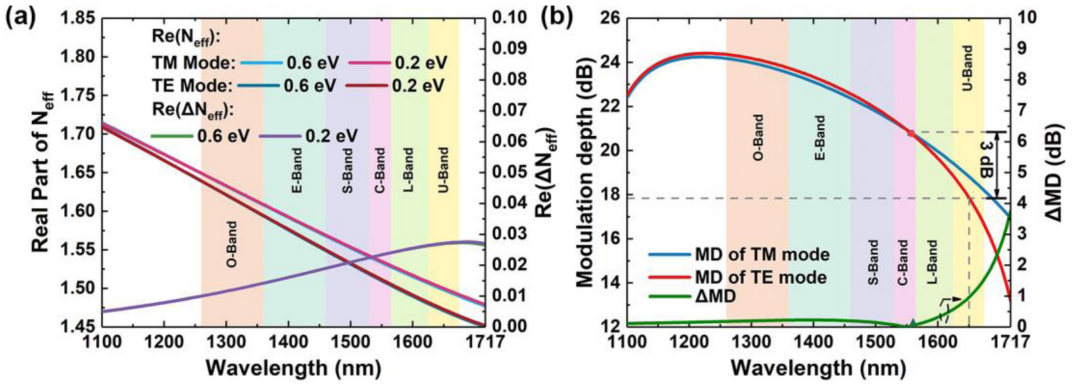

Fig. 8. (a) Re($N_{\rm eff}$) and Re($\Delta N_{\rm eff}$), (b) MD and ΔMD of TM and TE modes versus the incident wavelength at $\mu_{\rm c} = 0.2$ and 0.6 eV, respectively.

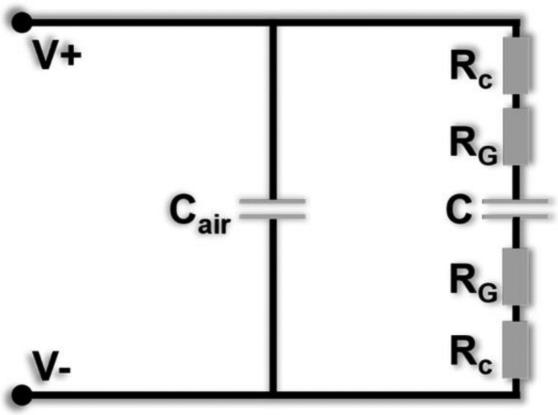

Fig. 9. Equivalent circuit for proposed graphene/SiN hybrid waveguide modulator.

mode than TM mode, which is unfavorable to broadband operation. If $\lambda = 1550$ nm is set to be the center wavelength, the optical 3 dB-bandwidth is from 1100 to 1645 nm for both polarizations, which covers the whole O- to L-band and part of U-band. Meanwhile, a low average ΔMD of 0.2 dB within this optical 3 dB-bandwidth is maintained, which implies the proposed modulator has a good polarization independency.

4. Performance and Discussion

The frequency characteristic of proposed modulator is studied by using the circuit model depicted in Fig. 9. Here, capacitance $C_{\rm air}$ is considered to exist between two electrodes and air, which is 12 fF [47]. The capacitance C that is composed of the two graphene layers and hBN isolation layer, consists of both the dielectric capacitance $C_{\rm D}$ and the quantum capacitor $C_{\rm Q}$. Assuming the graphene layer is undoped ($n_{\rm s} = 0$), then we have $C_{\rm Q} = 0$. Hence, the capacitance C can be described by the following capacitor model

$$C = \varepsilon_r \varepsilon_0 w_{ol} L/d \tag{7}$$

where $w_{\rm ol} = 1300$ nm is the overlap width between two graphene layers, $L = 200$ μm is the modulation length, $d = 10$ nm is the thickness of hBN, and $\varepsilon_{\rm r}$ is the dielectric constant of hBN layer. The contact resistance $R_{\rm c}$ induced by metal electrode contact and the graphene sheets resistance

TABLE 1
Comparison of Polarization-Insensitive Graphene Modulators at $\lambda = 1550$ nm.

Ref	Bandwidth (nm)	Re(ΔN_{eff})	MD (dB)	ΔMD (dB)	f_{3dB} (GHz)	E_{bit} (pJ/bit)
[39]	1500 - 1600	-	0.06	0	13.4	-
[40]	1500 -1600	-	0.08	0	80	-
[41]	1200 -1600	-	Mode A: 1.05 (dB/μm) Mode B: 1.13 (dB/μm) Mode C: 0.52 (dB/μm)	Min: 0.08 (dB/μm) Max: 0.61 (dB/μm)	95	0.1388
[42]	1530 -1565	~ 4.7×10^{-3}	TM mode: 14.875 TE mode: 14.475	0.4	30.2	2.98
[43]	1367 -1668	~ 0.5	TM mode: 22.26 TE mode: 22.38	0.12	6.1	7.80
[42]	1450 - 1650	~ 0.1	TM mode: 41.76 TE mode: 40.41	1.35	~ 100	-
[45]	1300 - 1800	1.2×10^{-3}	-	-	135.6	-
This	1100 - 1717	2.33×10^{-2}	TM mode: 20.940 TE mode: 20.936	4×10^{-3}	53	0.687

R_s contributes to the total resistance R_{total}. Here, R_{total} can be calculated by [16, 20]

$$R_{\text{total}} = 2R_s \times \frac{w_g}{L} + \frac{2R_c}{L} \tag{8}$$

where the effective graphene width w_g is the sum of overlapping width w_{ol} and the extending width. Here, the extending width refers to the part of graphene layer that connects to the electrode, and is set to be 500 nm. Hence, w_g is 1.8 μm. The sheet resistance R_s is 100 Ω/□ [10], and the contact resistance R_c is considered to be 150 Ω-μm [32]. Hence, we have a $R_{total} \approx 3.3$ Ω. The 3 dB-bandwidth (f_{3dB}) is primarily limited by the *RC* delay, which can be evaluated by

$$f_{3\text{dB}} = \frac{1}{2\pi R_{\text{total}} C_{\text{total}}} \tag{9}$$

When the chemical potential shifts from 0.2 to 0.6 eV, which corresponds an external voltage change of 1.734 V, we would have a f_{3dB} of 53 GHz. This relatively high frequency response is primarily owing to the low permittivity and small thickness of the isolation layer, as well as the short overlap length. To be mentioned, the large cross-section dimension of the waveguide due to the relatively small refractive index difference between the SiN and the cladding (compared with the SOI) leads to an inevitable increase in the width of the graphene layer, which is unfavorable to expand the bandwidth. f_{3dB} can be improved by using the SOI technique with higher refractive index difference and the adoption of isolation layer with a lower refractive index. The sheet resistance R_s and contact resistance R_c that are default values from the reference can be optimized, too [48]. With above confirmed parameters, the power consumption ($E_{bit} = C_{total}(\Delta U)^2/4$) is calculated to be 0.687 pJ/bit at $L = 200$ μm.

To better illustrate the characteristics of proposed work, the simulation results of reported polarization-insensitive graphene modulator are compared with those obtained from this graphene/SiN hybrid waveguide modulator at the optical wavelength 1550 nm. As listed in Table 1 below, the proposed modulator has the largest optical bandwidth and the excellent low ΔMD. Moderate MD and f_{3dB} shows a balanced performance. Besides, E_{bit} is smaller than most reported works, too.

To be more convincing, the high-frequency transmission of proposed graphene modulator is simulated by investigating the eye-diagram. The setup for simulation is shown in Fig. 10 below. The

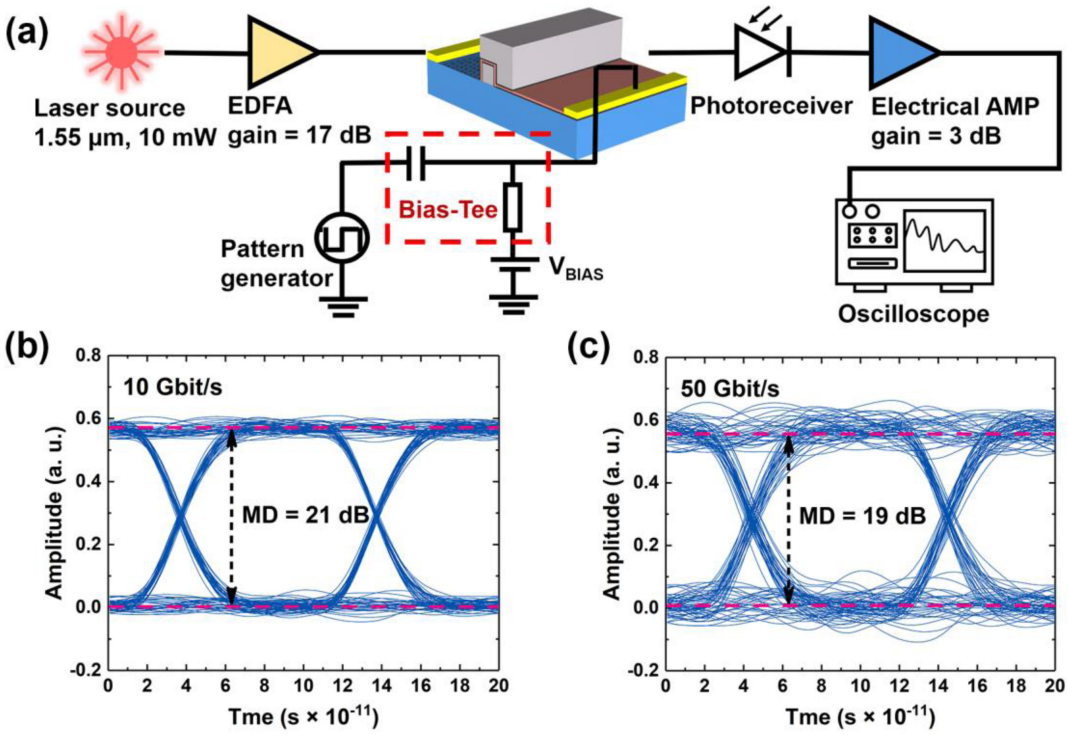

Fig. 10. Schematic diagram of (a) high-frequency transmission simulation, (b) and (c) are the eye diagram of $2^{31}-1$ PRBS transmission at data rates of 10 and 50 Gb/s.

graphene modulator is supposed to be driven by a non-return-to-zero (NRZ) signal that is generated by a pattern generator (PG). The PRBS code ($2^{31}-1$) is provided by PG at data rates of 10 Gb/s and 50 Gb/s, which cover the theoretical bandwidth expectation. The electrical driving signal is input with the radio frequency (RF) cable and bias-tree, as shown within the dashed line. An erbium doped fiber amplifier (EDFA) is adopted to amplify the light at the input of waveguide, compensating the optical power loss induced by the modulator. A high-frequency photodetector (PD) is used to collect the modulated light. The converted electrical signal is amplified (3 dB) and recorded by a digital sampling oscilloscope to observe the eye-diagram. The noise is supposed to be restrained by impedance matching between the PG electrical output and the device with a 50 Ω load. An extinction ratio varies from 21 dB at the data rate of 10 Gb/s to 19 dB at the data rate of 50 Gb/s. As has been reported [49, 50], to avoid dielectric breakdown, the bias voltage is unable to be over the Pauli blocking condition, which weakens the absorption effect. Besides, the resistance load may affect the extinction ratio due to its shunting the RF driving power, too. Though these simulated extinction ratios are ideal ones that are far too larger than practical values, it proves the functional feasibility of proposed modulator to some extent. Thereby, we believe that high-speed and practical polarization-insensitive graphene modulators can be expected with favorable fabrication.

The fabrication of proposed electro-absorption modulator may start with a commercial silica wafer. The bottom SiN rectangular substructure can be formed by sequentially conducting plasma-enhanced chemical vapor deposition (PECVD), surface mechanical chemical polishing, E-beam lithography, and plasma etching. Since the multilayer graphene stacks encapsulated in hBN and 3D graphene structure embedded in waveguide have been experimentally proved [51, 52], continuous multilayer graphene flakes coating on the rectangle SiN substructure uniformly both in the horizontal and vertical direction can be implemented. The graphene-covered region may be further defined by the E-beam lithography. The excess graphene on one side of the substructure will be removed. On the other side, the graphene flake extends 500 nm outwards and contacts with

the Au pad fabricated by thermal evaporation and lift-off process, forming the electrode. Finally, the top SiN layer can be fabricated by another PECVD, photolithography and plasma etching, forming the graphene-hBN-graphene heterostructure [53].

Alternatives can be adopted to further optimized the modulation performance, such as embedding more graphene layers into the SiN waveguide to improve the modulation depth. In this way, a better graphene-light field interaction can be constructed. According to our calculations, for the same waveguide dimension 660 nm $\times$ 660 nm, the modulation efficiency (ME) linearly increases with the number increment of graphene layers for both TE and TM mode. Meanwhile, $\triangle$ME will keep at a low level and can be further optimized by adjusting $\triangle h$ or $\triangle H$. Since a low contact resistance close to the theoretical limit has been reported [33], if the contact resistance R_c is 100 Ω, a f_{3dB} of 62 GHz and E_{bit} of 0.7 pJ/bit can be expected. Furthermore, if SiN waveguide core is replaced by high refractive index material, for example, silicon, the waveguide dimension can be significantly decreased to 300 nm $\times$ 300 nm, which promises a f_{3dB} of 177 GHz and E_{bit} of 0.3 pJ/bit.

5. Conclusion

To construct the polarization-insensitive modulation and enhance the interaction between graphene and optical mode, a broadband graphene/SiN hybrid waveguide electro-absorption modulator is proposed and comprehensively investigated. The polarization independency and deeper modulation is obtained by quasi-equal interaction between graphene flakes and optical modes in both the vertical and lateral direction. N_{eff}, Re($\triangle N_{eff}$), MPA, MD, and $\triangle$MD are investigated to optimize the waveguide geometry parameters. When the external bias voltage shifts from 0.217 to 1.951 V, the MD for TM and TE mode are 20.940 and 20.936 dB, respectively. Low $\triangle$MD of 0.2 dB and Re($\triangle N_{eff}$) of 2.33 $\times$ 10^{-2} is active within an optical 3 dB-bandwidth of 1100 to 1645 nm. An ultra-low $\triangle$MD of 4 $\times$ 10^{-3} dB is retained at $\lambda = 1.55$ μm. The insertion loss is estimated to be 1.425 dB. Calculations show that f_{3dB} of 53 GHz and E_{bit} of 0.687 pJ/bit at a modulation length of 200 μm can be obtained. The proposed modulator has merits of compact footprint, broadband operation and polarization insensitivity. It has potentials in on-chip signal processing.

Acknowledgment

The authors thank for the simulation support from the researchers from the Institute of Semiconductor, Chinese Academy of Sciences.

References

[1] D. Marris-Morini *et al.*, "Recent progress in high-speed silicon-based optical modulators," *Proc. IEEE*, vol. 97, no. 7, pp. 1199–1215, Jul. 2009.
[2] A. J. Mercante, D. L. K. Eng, M. Konkol, P. Yao, S. Shi, and D. W. Prather, "Thin $LiNbO_3$ on insulator electro-optic modulator," *Opt. Lett.*, vol. 41, no. 5, pp. 867–869, 2016.
[3] D. Feng *et al.*, "High speed gesi electro-absorption modulator at 1550 nm wavelength on SOI waveguide," *Opt. Exp.*, vol. 20, no. 20, pp. 22224–22232, 2012.
[4] G. Sinatkas, A. Pitilakis, D. C. Zografopoulos, R. Beccherelli, and E. E. Kriezis, "Transparent conducting oxide electro-optic modulators on silicon platforms: A comprehensive study based on the drift-diffusion semiconductor model," *J. Appl. Phys.*, vol. 121, no. 2, pp. 23109–23121, 2017.
[5] D. Pérez-Galacho, D. Marris-Morini, R. Stoffer, E. Cassan, and L. Vivien, "Simplified modeling and optimization of silicon modulators based on free-carrier plasma dispersion effect," *Opt. Exp.*, vol. 24, no. 23, pp. 26332–26337, 2016.
[6] M. Fan, H. Yang, P. Zheng, G. Hu, B. Yun, and Y. Cui, "Multilayer graphene electro-absorption optical modulator based on double-stripe silicon nitride waveguide," *Opt. Exp.*, vol. 25, no. 18, pp. 21619–21629, 2017.
[7] J. F. Bauters, M. J. R. Heck, D. D. John, J. S. Barton, and J. E. Bowers, "Planar waveguides with less than 0.1 db/m propagation loss fabricated with wafer bonding," *Opt. Exp.*, vol. 19, no. 24, pp. 24090–24101, 2011.
[8] J. Feng and R. Akimoto, "A three-dimensional silicon nitride polarizing beam splitter," *IEEE Photon. Technol. Lett.*, vol. 26, no. 7, pp. 706–709, 2014.
[9] X. Zhang, Y. Zhang, C. Xiong, and B. J. Eggleton, "Correlated photon pair generation in low-loss double-stripe silicon nitride waveguides," *J. Opt.*, vol. 18, no. 7, pp. 74016–74021, 2016.
[10] L. Abdollahi Shiramin and D. Van Thourhout, "Graphene modulators and switches integrated on silicon and silicon nitride waveguide," *IEEE J. Sel. Topics Quantum Electron.*, vol. 23, no. 1, pp. 94–100, 2016.

[11] N. Gruhler, C. Benz, H. Jang, J. H. Ahn, R. Danneau, and W. H. P. Pernice, "High-quality si_3n_4 circuits as a platform for graphene-based nanophotonic devices," *Opt. Exp.*, vol. 21, no. 25, pp. 31678–31689, 2013.
[12] A. K. Geim and K. S. Novoselov, "The rise of graphene," *Nature Mater.*, vol. 6, no. 3, pp. 183–191, 2009.
[13] F. Schwierz, "Graphene transistors," *Nature Nanotechnol.*, vol. 5, no. 7, pp. 487–496, 2010.
[14] J. Kusuma, R. G. Balakrishna, S. Patil, M. S. Jyothi, H. R. Chandan, and R. Shwetharani, "Exploration of graphene oxide nanoribbons as excellent electron conducting network for third generation solar cells," *Sol. Energy Mater. Sol. Cells*, vol. 183, pp. 211–219, 2018.
[15] P. Avouris, Z. Chen, and V. Perebeinos, "Carbon based electronics," *Nature Nanotechnol.*, vol. 2, no. 10, pp. 605–615, 2007.
[16] F. Bonaccorso, T. Hasan, Z. Sun, and A. C. Ferrari, "Graphene photonics and optoelectronics," *Nature Photon.*, vol. 4, no. 9, pp. 611–622, 2010.
[17] K. I. Bolotin *et al.*, "Ultrahigh electron mobility in suspended graphene," *Solid State Commun.*, vol. 146, no. 9, pp. 351–355, 2008.
[18] R. R. Nair *et al.*, "Fine structure constant defines visual transparency of graphene," *Science*, vol. 320, no. 5881, pp. 1308–1308, 2008.
[19] K. F. Mak, M. Y. Sfeir, Y. Wu, C. H. Lui, J. A. Misewich, and T. F. Heinz, "Measurement of the optical conductivity of graphene," *Phys. Rev. Lett.*, vol. 101, no. 19, pp. 196405–196408, 2008.
[20] B. Sensale-Rodriguez *et al.*, "Broadband graphene terahertz modulators enabled by intraband transitions," *Nature Commun.*, vol. 3, no. 1, 2012, Art. no. 780.
[21] Y. Hu *et al.*, "Broadband 10 Gb/s operation of graphene electro-absorption modulator on silicon," *Laser Photon. Rev.*, vol. 10, no. 2, pp. 307–316, 2016.
[22] M. Mohsin, D. Schall, M. Otto, A. Noculak, D. Neumaier, and H. Kurz, "Graphene based low insertion loss electro-absorption modulator on SOI waveguide," *Opt. Exp.*, vol. 22, no. 12, pp. 15292–15297, 2014.
[23] H. Dalir, Y. Xia, Y. Wang, and X. Zhang, "A thermal broadband graphene optical modulator with 35 GHz speed," *ACS Photon.*, vol. 3, no. 9, pp. 1564–1568, 2016.
[24] A. Phatak, Z. Z. Cheng, C. Y. Qin, and K. Goda, "Design of electro-optic modulators based on graphene-on-silicon slot waveguides," *Opt. Lett.*, vol. 41, no. 11, pp. 2501–2504, 2016.
[25] M. Liu *et al.*, "A graphene-based broadband optical modulator," *Nature*, vol. 474, no. 7349, pp. 64–67, 2011.
[26] M. Liu, X. Yin, and X. Zhang, "Double-layer graphene optical modulator," *Nano Lett.*, vol. 12, no. 3, pp. 1482–1485, 2012.
[27] C. T. Phare, Y.-H. Daniel Lee, J. Cardenas, and M. Lipson, "Graphene electro-optic modulator with 30 GHz bandwidth," *Nature Photon.*, vol. 9, no. 8, pp. 511–514, 2015.
[28] M. Iqbal, Z. Zheng, and J. S. Liu, "Slot optical waveguide usage in forming passive optical devices," *Recent Pat. Nanotechnol.*, vol. 6, no. 1, pp. 73–77, 2012.
[29] K. Kim, J.-Y. Choi, T. Kim, S.-H. Cho, and H.-J. Chung, "A role for graphene in silicon-based semiconductor devices," *Nature*, vol. 479, no. 7373, pp. 338–344, 2011.
[30] J. A. Schuller, E. S. Barnard, W. Cai, Y. C. Jun, J. S. White and M. L. Brongersma, "Plasmonics for extreme light concentration and manipulation," *Nature Mater.*, vol. 9, no. 3, pp. 193–204, 2010.
[31] Q. Bao *et al.*, "Broadband graphene polarizer," *Nature Photon.*, vol. 5, no. 7, pp. 411–415, 2011.
[32] H. Zhong *et al.*, "Realization of low contact resistance close to theoretical limit in graphene transistors," *Nano Res.*, vol. 8, no. 5, pp. 1669–1679, 2015.
[33] Y. Kim and M.-S. Kwon, "Electroabsorption modulator based on inverted-rib-type silicon waveguide including double graphene layers," *J. Opt.*, vol. 19, no. 4, pp. 45804–45811, 2017.
[34] Y. Ding, X. Guan, X. Zhu, H. Hao, and S. Xiao, "Effective electro-optic modulation in low-loss graphene-plasmonic slot waveguides," *Nanoscale*, vol. 9, no. 40, pp. 15576–15581, 2017.
[35] L. Ye, K. Sui, Y. Zhang, and Q. H. Liu, "Broadband optical waveguide modulators based on strongly coupled hybrid graphene and metal nanoribbons for near-infrared applications," *Nanoscale*, vol. 11, no. 7, pp. 3229–3239, 2019.
[36] Hanson and G. W., "Dyadic green's functions and guided surface waves for a surface conductivity model of graphene," *J. Appl. Phys.*, vol. 103, no. 6, pp. 64302–64309, 2007.
[37] C. Hwang *et al.*, "Fermi velocity engineering in graphene by substrate modification," *Sci. Rep.*, vol. 2, no. 1, pp. 590–593, 2012.
[38] M.-S. Kwon, "Discussion of the epsilon-near-zero effect of graphene in a horizontal slot waveguide," *IEEE Photon. J.*, vol. 6, no. 3, Jun. 2014, Art. no. 6100309.
[39] Z. Yang, R. Lu, S. Cai, Y. Wang, Y. Zhang, X. Wang, and Y. Liu, "A CMOS-compatible and polarization-insensitive graphene optical modulator," *Opt. Commun.*, vol. 450, pp. 130–135, 2019.
[40] Z. Yang, R. Lu, Y. Wang, S. Cai, Y. Zhang, X. Wang, and Y. Liu, "A fabrication-friendly graphene-based polarization insensitive optical modulator," *Optik*, vol. 182, pp. 1093–1098, 2019.
[41] M. Shirdel and M. A. Mansouri-Birjandi, "Broadband graphene modulator based on a plus-shaped plasmonic slot waveguide," *Appl. Opt.*, vol. 58, no. 30, pp. 8174–8179, 2019.
[42] X. Hu and J. Wang, "Design of graphene-based polarization-insensitive optical modulator," *Nanophotonics*, vol. 7, no. 3, pp. 651–658, 2018.
[43] Y. Xu, F. Li, Z. Kang, D. Huang, X. Zhang, H.-Y. Tam, and P. Wai, "Hybrid graphene-silicon based polarization-insensitive electro-absorption modulator with high-modulation efficiency and ultra-broad bandwidth," *Nanomaterials*, vol. 9, no. 2, pp. 157–171, 2019.
[44] S. W. Ye *et al.*, "Polarization independent modulator by partly tilted graphene induced electro-absorption effect," *IEEE Photon. Technol. Lett.*, vol. 29, no. 1, pp. 23–26, Jan. 2016.
[45] X. H. Zou *et al.*, "Polarization-insensitive phase modulators based on an embedded silicon-graphene-silicon waveguide," *Appl. Sci.-Basel*, vol. 9, no. 3, pp. 429–436, 2019.
[46] Y. Maegami, M. Okano, G. Cong, M. Ohno and K. Yamada, "Completely CMOS compatible SiN-waveguide-based fiber coupling structure for Si wire waveguides," *Opt. Exp.*, vol. 24, no. 15, pp. 16856–16865, 2016.

[47] Y. Hu *et al.*, "High-speed silicon modulator based on cascaded microring resonators," *Opt. Exp.*, vol. 20, no. 14, pp. 15079–15085, 2012.
[48] P. Zheng, H. Yang, M. Fan, G. Hu, R. Zhang, B. Yun, and Y. Cui, "A hybrid plasmonic modulator based on graphene on channel plasmonic polariton waveguide," *Plasmonics*, vol. 13, no. 6, pp. 2029–2035, 2018.
[49] V. Sorianello *et al.*, "Optical pre-emphasis by cascaded graphene electro absorption modulators," *IEEE Photon. Technol. Lett.*, vol. 31, no. 12, pp. 955–958, Dec. 2019.
[50] M. A. Giambra *et al.*, "High-speed double layer graphene electro-absorption modulator on soi waveguide," *Opt. Exp.*, vol. 27, no. 15, pp. 20145–20155, 2019.
[51] Q. Huang and K. S. Chiang, "Polarization-insensitive ultra-broadband mode filter based on a 3D graphene structure buried in an optical waveguide," *Optica*, vol. 7, no. 7, pp. 744–745, 2020.
[52] F. Pizzocchero *et al.*, "The hot pick-up technique for batch assembly of van der Waals heterostructures," *Nature Commun.*, vol. 7, no. 1, pp. 11894–11903, 2016.
[53] M. Schaepkens, T. E. F. M. Standaert, N. R. Rueger, P. G. M. Sebel, G. S. Oehrlein, and J. M. Cook, "Study of the siO_2 to Si_3N_4 etch selectivity mechanism in inductively coupled fluorocarbon plasmas and a comparison with the SiO_2 to Si mechanism," *J. Vac. Sci. Technol. A*, vol. 17, no. 1, pp. 26–37, 1999.